Validation of Meteorological Models and Parametrizations with Observations of the PYREX Field Experiment

Ph. Bougeault, I. Beau, and J. Stein
Météo-France, CNRM (31057 Toulouse France)

1 Introduction

Twenty years have passed since Lilly (1972) identified the orographic drag as a major sink of atmospheric momentum, leading to continued development of research on mountain influence on the atmosphere. During these two decades, his idea has been largely confirmed by experimental, numerical and theoretical work. The study of orographic effects has emerged as one of rich and still largely unexplored phenomenology, exciting theoretical problems, ideal test-bed for new instrumentation, and the key to drastic improvements of numerical forecasts, both at meso and larger scales, including climate models. It is therefore no surprise if the Météo-France proposal to conduct a major field study of the dynamical influence of the Pyrénées mountains on the atmospheric flow has received a strong support from many agencies and institutes, and attracted several scientists from the near-by countries. A list of these agencies is given in the acnowledgments section and a list of acronyms may be found in Table 1. The resulting field program, called PYREX, was described by Bougeault et al.(1990), and conducted in October and November, 1990. The aim of the present paper is to give a broad description of the experimental results, encountered phenomenology, available data-sets, and to discuss the opportunities of validation of meso-scale models and parametrizations offered by these observations. An extended version of this paper, including more experimental results, is to be submitted shortly to *Annales Geophysicae* (Bougeault et al., 1992) .

The motivations of the different participants were discussed in detail by Bougeault et al. (1990). In summary, they range from a better knowledge of the phenomenology of mean and turbulent wind and pressure patterns in the vicinity of the Pyrenean range, to an accurate, possibly operational, numerical modelling of these patterns, through an improved

Acronym	Full Name	Affiliation
CNES	Centre national d'études spatiales	Minist. Research (France)
CNRM	Centre National de Recherches Météorologiques	Météo-France and CNRS
CNRS	Centre National de la Recherche Scientifique	Minist. Research (France)
CRPE	Centre de Recherche en Physique de l'Environnement	CNRS and CNET
DLR	Deutsche Forschungsanstalt für Luft und Raumfahrt	Minist. Res. (Germany)
EDF	Electricité de France	Independant agency
IGN	Institut Géographique National	Independant Agency
INM	Instituto National de Meteorologià (Spanish Weather Service)	Minist. Transp. (Spain)
INSU	Institut National des Sciences de l'Univers	CNRS
LA	Laboratoire d'Aérologie	CNRS and Toulouse University
LAMP	Laboratoire de Météorologie Physique	CNRS and Clermont-Ferrand University
LMD	Laboratoire de Météorologie Dynamique	CNRS
LSEET	Laboratoire de Sondages Electromagnétique de l'Environnement Terrestre	CNRS and University Toulon
Météo-France	French Weather Service	Minist. Transp. (France)
SA	Service d'Aéronomie	CNRS and Paris University
UIB	Department of Physics	University of Balearic Islands
UV	Department of Physics	University of Valladolid

Table 1: List of Acronyms

Instrument	Location	Responsible Institute
15 Auto stations	Central transect	CNRM
3 Auto stations	Baraignes, ..	EDF
2 Sodars	Baraignes, Espiaube	EDF
Sodar	Lannemezan	CRPE
Sodar	Zaragoza	INM
Sodar	Tortosa	UV
VHF Profiler	Lannemezan	LSEET
VHF Profiler	Saint-Larry	CNRM
VHF Profiler	Ainsa	LAMP
UHF Profiler	Lannemezan	CRPE
Balloons	Pic du Midi Port la Nouvelle Cap Creus	LA and CNRM
Falcon		DLR
Fokker 27 ARAT		CNES, INSU, Météo-France, IGN
Piper Aztec		CNRM
MerlinIV		CNRM

Table 2: A list of the facilities operating during PYREX

representation of the underlying dynamical processes, in connection with the most recent theories of orographic flows. A variety of meteorological phenomena are created by the Pyrénées: Foehn effects on either side of the range, downslope windstorms, regional winds farther in the plain, blocking, etc... A common problem to understand these dynamics, relies on a *quantitative appraisal of the momentum budget*, which was also precisely the type of information needed to better understand how the retardation effect of the mountain is felt by the atmosphere at larger scales. There was therefore a high convergence of scientific interests, justifying a cooperative experimental program. However, the difficulty of deriving a *reliable* momentum budget from measurements only is well known, and it was felt more adequate to use *numerical models* to achieve this result. This resulted, from the beginning of the planning phase, in a high level of cooperation between the modelling and experimental approaches. The measurements were organized not only to document some of the most important terms of the momentum budget, such as the pressure drag and wave momentum fluxes, but also to validate other aspects of meso-beta scale numerical simulations. Those numerical results in turn are to be used, *under the control of existing observations*, to derive the missing terms of the momentum budget over the instrumented areas, and *all* the terms of this budget over adjacent areas, or during periods when no special observations exist. This use of models as *numerical laboratories* has been illustrated in the past by the so-called large-eddy-simulation approach. Recently, it has been applied by Hoinka and Clark(1991), and Clark and Miller(1991) to flows over the Alps. These last studies are very close in essence to the foreseen scientific use of the PYREX data, but we think we can improve on their results, since we were fortunate enough to observe a wide variety of situations, with a large number of quality systems.

Section 2 will describe briefly the experimental set-up, the encountered situations and the main existing data-sets. This will be followed by a discussion of the best Southern case (IOP 3). Experimental results will be presented and compared with numerical results in Section 3. We will try to derive some preliminary conclusions concerning the momentum budget in Section 4. Section 5 will report on some recent comparisons between the ECMWF and Météo-France gravity wave drag parametrizations and our results.

2 Overview of Available Data

To reach the above mentioned objectives, it was necessary to use both an infrastructure of ground-based measurements, operating either continuously or on alert, and a fleet of research

aircraft and constant-level balloons flying in coordination. A synoptic view of the ground infrastructure is given in Fig.1, with a list of responsible institutes in Table 2. We used the concept of Intensive Observation Period (IOP in the following), corresponding to the activation of regular upper-air soundings, and to the intensification of basic measurements. The IOPs centered in time around aircraft operations. The aircraft flight plans were organized depending on specific missions. There were four different missions, corresponding to the documentation of the main mountain wave/lee wave system, and to the documentation of the mean flow and turbulence in either of the three regional winds caused by the Pyrénées: *Autan, Tramontana*, and *Cierzo*. The climatological domains of extension of these winds are shown in Fig.1. We were fortunate to encounter situations comparable to the climatology for all four types of missions, during the two months duration (October and November 1990) of the experiment. There were 10 IOPs, **totalling** 15 days of intensive measurements. A summary of the IOPs starting and finishing times, types of event, and aircraft/balloons operations is given in Table 3.

2.1 Permanent surface networks

Regularly operating surface networks of the PYREX area include different types, ranging from the main stations of the WMO network, regularly staffed and operating continuously, to stations of local interest, and a large number of fully automated stations. With over 170 permanent stations, the PYREX area is probably one of the most densely covered in the world by surface meteorological measurements, which made it an ideal candidate for such a field study. However, some gaps were noted in the permanent network, which justified the installation of 3 additionnal surface stations by EDF in the Pyrenean foothills. During the field phase all stations operated as usual, generating a large diversity in the periodicity, nature and format of their measurements. In order to ease further interpretation work, the format and periodicity of all the data sources have been normalized in the PYREX data base. Most data are available on a half hourly basis. All stations reported temperature, humidity, wind strength and direction, and several of them reported pressure. In addition, a large number of stations reported informations on gust speed and direction, rainfall, radiation, and sensible weather. All these informations have been kept in the Data Base to facilitate the interpretation. A quick look atlas of these surface measurements, containing a discussion of the validation procedures, has been prepared by Champeaux and Péris (1991).

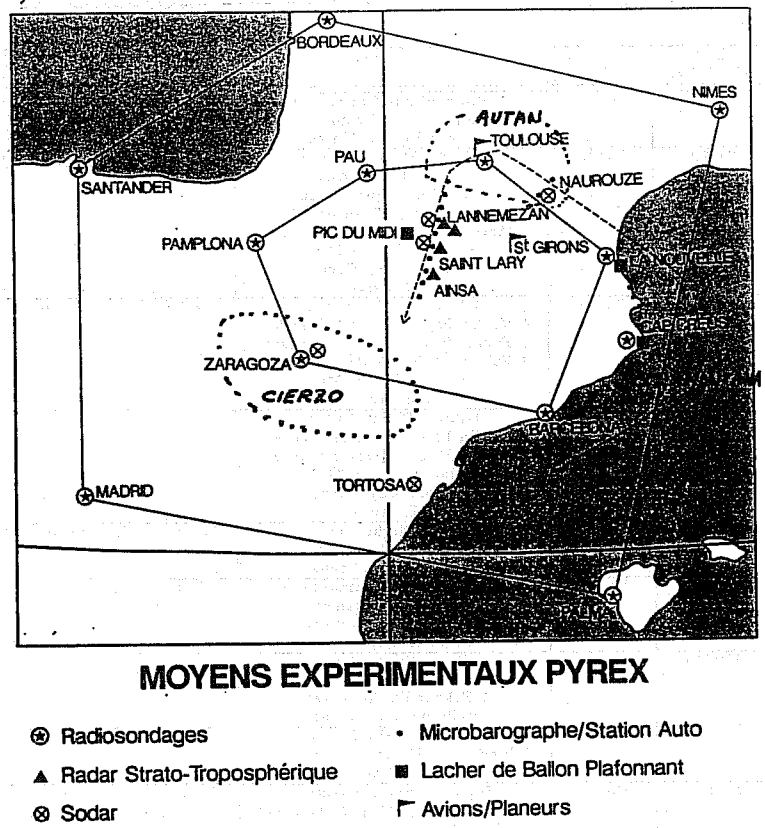

Fig.1: Synoptic view of the ground infrastructure during PYREX.

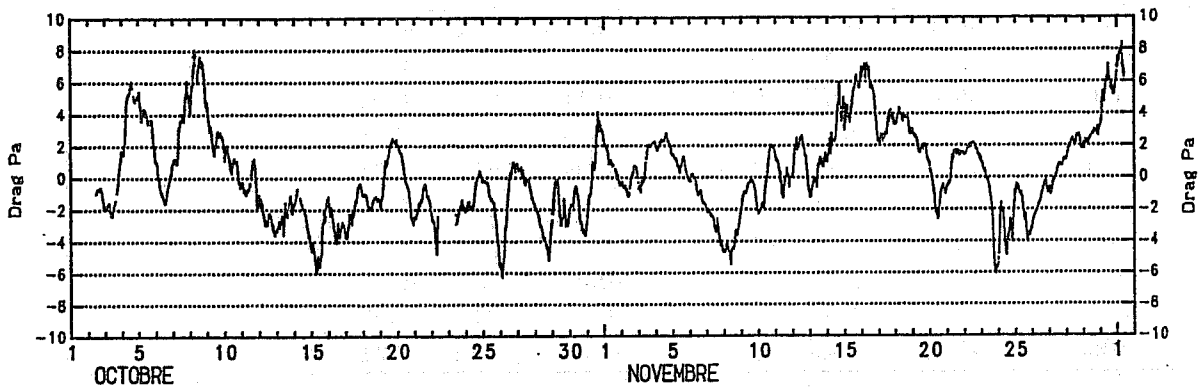

Fig.2: The 2 months time series of the surface pressure drag computed from measurements of the CNRM portable network (from Puech et al., 1991).

POI	Start MMJJHH	End MMJJHH	Synoptic wind	Operations	Comments
1	100418	100518	North	1 Piper Flight Tramontana 1 Merlin Flight Tramontana Balloons Port la Nouvelle	
2	101118	101406	South South	2 Piper Flights Autan 1 Fokker Flight Autan 1 Merlin Flight Autan 1 Fokker Central Transect Flight 1 Merlin Central Transect Flight Balloons Pic du Midi Balloons Cap Creus Sailplanes	
3	101418	101512	South	1 Piper Flight Autan 1 Merlin Flight Central Transect 1 Fokker Flight Central transect 1 Falcon Flight Central transect Balloons Pic du Midi Sailplanes	Best case of lee waves from South
4	102018	102118	South	1 Piper Flight Autan 1 Merlin Flight Central transect 1 Fokker Flight Central transect Balloons Pic du Midi Balloons Cap Creus Sailplanes	
5	102518	102612	South	1 Piper Flight Autan 1 short Merlin Flight Balloons Cap Creus	Front crossing the area during operations
6	110318	110518	North	1 Piper Flight Tramontana 2 Merlin Flights Tramontana 2 Fokker Flights Tramontana Balloons Cap Creus	Tramontana weakens during 2nd day
7	110618	110718	South	1 Piper Flight Autan 1 Merlin Flight Autan 1 Fokker Flight Autan Balloons Cap Creus	
8	111118	111218	North	1 Piper Flight Cierzo 1 Merlin Flight Central transect Balloons Cap Creus	
9	111406	111618	North	2 Flights Piper Tramontana 3 Merlin Flights Central transect 3 Fokker Flights Central transect 3 Falcon Flights Central transect Balloons Port la Nouvelle	Best case of lee waves from North Strongest Tramontana
10	112818	113018	North	2 Piper Flights Cierzo 2 Merlin Flights Cierzo 2 Fokker Flights Cierzo Balloons Port la Nouvelle	Best Cierzo on 2nd day

Table 3: List of IOPs and operations

Altitude m	F_y $10^5 N m^{-1}$	M_y $10^{10} N$	D_y Pa	F_x $10^5 N m^{-1}$	M_x $10^{10} N$	D_x Pa
11700	-0.35	-1.05	-0.19	-0.31	-0.92	-0.16
11100	-0.37	-1.10	-0.20	-0.43	-1.28	-0.23
10500	-0.72	-2.17	-0.39	0.11	0.33	0.06
10000	-0.32	-0.94	-0.17	0.26	0.77	0.14
9300	-0.34	-1.03	-0.18	-0.08	-0.23	-0.04
8000	-0.48	-1.43	-0.25	-0.12	-0.36	-0.06
6000	-0.15	-0.46	-0.09	0.08	0.24	0.04
5000	-0.97	-2.91	-0.53	-0.08	-0.23	-0.04
4200	-1.07	-3.21	-0.71	-0.09	-0.28	-0.06
4000	-1.48	-4.43	-0.81	-0.38	-1.14	-0.21

Table 4: The net force per unit length perpendicular to the track (F_x, F_y), the drag per unit area (D_x, D_y), and the total drag (M_x, M_y). The total drag is computed assuming a West-East extension of the Pyrénées of $300km$ (Courtesy of K.P. Hoinka).

2.2 CNRM portable network and drag computation

An extra network of 15 automated surface stations was operated by CNRM during the field phase. Those stations have been installed at selected mountain sites of known altitudes, along a transect perpendicular to the main range, as shown in Fig.1. This will be called in the following the *central transect*. In addition to the usual meteorological measurements, high quality pressure measurements were made at those stations, in order to determine the pressure drag across the range. A quick look atlas of these data has been prepared by Puech et al.(1991). The Davies and Philipps (1985) procedure was used to compute every ten minutes the drag per unit area (units Pa) by the formula

$$D = L^{-1} \int_{z_{bottom}}^{z_{top}} \Delta p(z) dz,$$

where $\Delta p(z)$ is the pressure difference between the two mountain sides at height z, retrieved from the raw data by spline interpolation, and L the length of the instrumented transect. This method was chosen because it operates with the observed pressure only (no reduction of the pressure to a standard level), and takes full advantage of the good relative accuracy of the sensors. Since the Pyrenean range is roughly two-dimensional, this value is thought to be representative of the pressure drag in the direction of the main transect in the mountain central part. It is probably higher than the pressure drag per unit area on the whole of the mountain range, and gives no information on the pressure drag in the direction parallel to the range (i.e. perpendicular to the transect). It will be the task of numerical modelling to derive the correspondence between this observed value and other determinations of the drag (see Section 4). The two-months observed drag time series, which constitutes one of the major experimental results, is shown in Fig.2. It ranges from -7 to $+8Pa$. Its algebraic mean value is $0.2Pa$, and its absolute mean value is $2.2Pa$. This indicates that the Pyrenean range is indeed a major sink of meridional momentum for the atmospheric flow. As expected, the time variations of the drag are very much correlated with the synoptic wind variations. We also found a weak diurnal cycle ($0.4Pa$ amplitude).

2.3 Upper air soundings

For the purpose of the experiment, the regular sounding network was upgraded to 12 sites in the PYREX area (see Fig.1). The soundings were organized in two arrays. The outer array is convenient to estimate meso-alpha scale quantities, whereas the inner array, composed of stations in the immediate vicinity of the range, is convenient to sample the meso-beta scale features of the orographic influence. Soundings of the inner array are kept in the

Data Base with the maximum available vertical resolution, whereas for those of the outer array, we have retained the significant and standard levels only. The soundings were not activated outside the Intensive Observation Periods (IOPs), except the normal operation of the WMO network. During the IOPs, they were made at 00, 06, 12, and 18 GMT. Most of these soundings were transmitted in real time on the GTS, and entered the assimilation cycle of Météo-France operational forecasting suite. The total number of soundings received, validated, and archived into the Pyrex Data Base is 720.

2.4 Acoustic sounders

Five acoustic sounding systems (Sodars) were implemented continuously during the experiment at $15min$ time resolution (see Fig.1). Some of them were located at places adequate to follow the *Cierzo* and *Autan* wind evolutions. Others were located on the main transect, at places of interest to document the ground manifestation of the mountain waves. The Sodars provided measurements of the low-level wind profiles, nominally from about 50 to 500 meters above the instrument. However the performances were in general inferior when the wind was strong, because of the antenna noise increase. For technical reasons, the data of the Tortosa Sodar are not usable. Carissimo et al.(1991) contains some quick look of the two sodars operated by EDF.

2.5 Wind profilers

Four profilers of the Météo-France/INSU research network (Petitdidier et al., 1986) have been used for the experiment. They were located on three sites along the main transect, on either side of the range and very close to the crest. The north site (Centre de Recherches Atmosphériques at Lannemezan) had two colocated profilers, covering different ranges of altitudes. The two other sites had more recent instruments with an ability to cover various ranges of altitudes, depending on the operating mode (3 modes were available, low resolution, high resolution, and "coded", a special feature that improves the resolution). The nominal requirements for the experiment called for profiles of the three components of the wind every twelve minutes during the IOPs, with alternating vertical resolutions of $375m$ (up to $12km$) and $2250m$ (up to $18km$). Those were generally not met, because the profilers were prototype research instruments, with limited power. As a consequence, the measurements were often limited by ground echos and by several technical problems. We have decided to retain formally in the data base the nominal time and space resolutions during the IOPs, and to assign to each data a quality code varying from 0 to 8, depending on the signal/noise

ratio. The data are also available outside the IOPs for the central site, at a time resolution of 1 hour. The performances of the profilers vary widely from day to day and from site to site, but despite the above mentionned problems, there are many valuable data, and we plan to perform several model/profilers and pressure drag/profilers comparisons.

2.6 Constant level balloons

The constant-level balloons described by Benech et al. (1987) were operated to obtain air trajectories, and *in situ* measurements of pressure, temperature and moisture. Three launching sites were used (Fig.1). One at Pic du Midi (close to the highest point of the central transect) was operated in case of lee waves on the northern side of the range. The balloons from this site were tracked by a radar located in Lannemezan. Their nominal flight height ranged from 3000 to $5000m$. Two other sites at Port la Nouvelle (France) and Cap Creus (Spain), on the eastern side of the range, were used to obtain low-level trajectories (400 to $1500m$ height a.s.l.) in the flow deviated laterally by the range. Trajectories tracked from one reception site usually are about $100km$ long, while trajectories reconstituted from both reception sites (the optimal situation) reach $200km$ in several cases, which is well beyond the present day expectations for such an experiment. Generally speaking, the balloon experiment was very successful, and provided reference data for the horizontal wind and the air-mass trajectories, which are very useful to assess the value of other types of measurements. The balloon data have been summarized by Koffi et al. (1991a, 1991b).

2.7 Aircraft measurements

Four research airplanes have been used for Pyrex missions. Those are the Fokker 27 ARAT (Avion de Recherche Atmosphérique et de Télédétection), operated by a group of french institutes (CNES, INSU, Météo-France, and IGN, see list of acronyms), the Merlin IV and the Piper-Aztec of Météo-France, and the Falcon of DLR. The Fokker, Merlin, and Falcon aircraft performed both turbulence and mean flow measurements, while the Piper measured only mean flow parameters. **Besides wind,** temperature, and moisture, which were the most needed measurements, additional measurements were made: Radiation in most cases, microphysics for the Merlin and Fokker, and Lidar for the Fokker (see below). There were two intercomparison flights between the french aircrafts during the experiment. These flights helped to resolve small discrepancies between the measurements, and to prepare a synthetic aircraft data-set, now available in the Data Base in a unified format. Three different types of data may be used: (i) 10 seconds averaged data for all parameters and all flights; (ii) 1 second

data for all parameters, restricted to the flight legs above the central transect, (for a more detailed documentation of the lee waves); (iii) elaborate turbulence quantities, computed from high frequency data for several flight legs (for comparison with model parametrization results).

The flight plans were organized in missions focusing on either of the experimental objectives. The *Autan* mission called for the Merlin, Fokker, and Piper executing coordinated flights in the geographical area of this wind. The *Tramontana* and *Cierzo* missions were fairly comparable, but in different geographical locations. These flights were focusing on detailed mean flow and turbulence measurements at three levels inside the Atmospheric Boundary Layer, allowing for an overpass of the area with the lidar scanning down to explore the top of the ABL. The aim was to obtain accurate measurements of the turbulent fluxes, and to interpret these fluxes in connection with possible organized structures (rolls), and the mesoscale forcing. In these three types of missions, there were no high altitude measurements, and the Falcon was not used. On the other hand, the *Central Transect* mission called for the Falcon joining the Fokker and Merlin in a coordinated flight above the mountain, while the Piper was executing alone the same flight as in the other three missions, depending on the situation. The Fokker and Falcon flight plans were fairly classical, crossing the main range several times, and flying right over the CNRM portable network, in order to estimate the wave momentum flux. The Merlin was assigned a more complicated flight plan, made of legs parallel to the main range, at different elevations and distances from the crest. The pilots had been asked to fly as low as it was reasonnably possible, to try to document the atmospheric boundary layer (ABL) over a high mountain. However, turbulence was only rarely encountered in these flights, indicating that the mountain ABL is very shallow. Another objective of this flight pattern was to assess the variability of the flow along the range and to study how the 3D perturbations created by individual peaks are smoothed out in altitude to generate a simpler 2D pattern. We believe that, despite the absence of turbulence, this dataset is one of the most original ever acquired over mountainous areas, and opens interesting opportunities to derive the mountain effective roughness, via indirect methods (comparison with model predicted winds, for instance). A schematic illustration of the coordinated flight plans for the Central Transect mission in a case of northern flow is given in Fig.3. This pattern was actually flown during IOP 9. The list of the available flights is given in Table 3. The flight logs of the on-board scientists have been published by Attié et al.(1991).

Thanks to a large number of low level turbulence measurements, accurate determinations of the surface friction over the sea were also possible during PYREX. Most of these data were

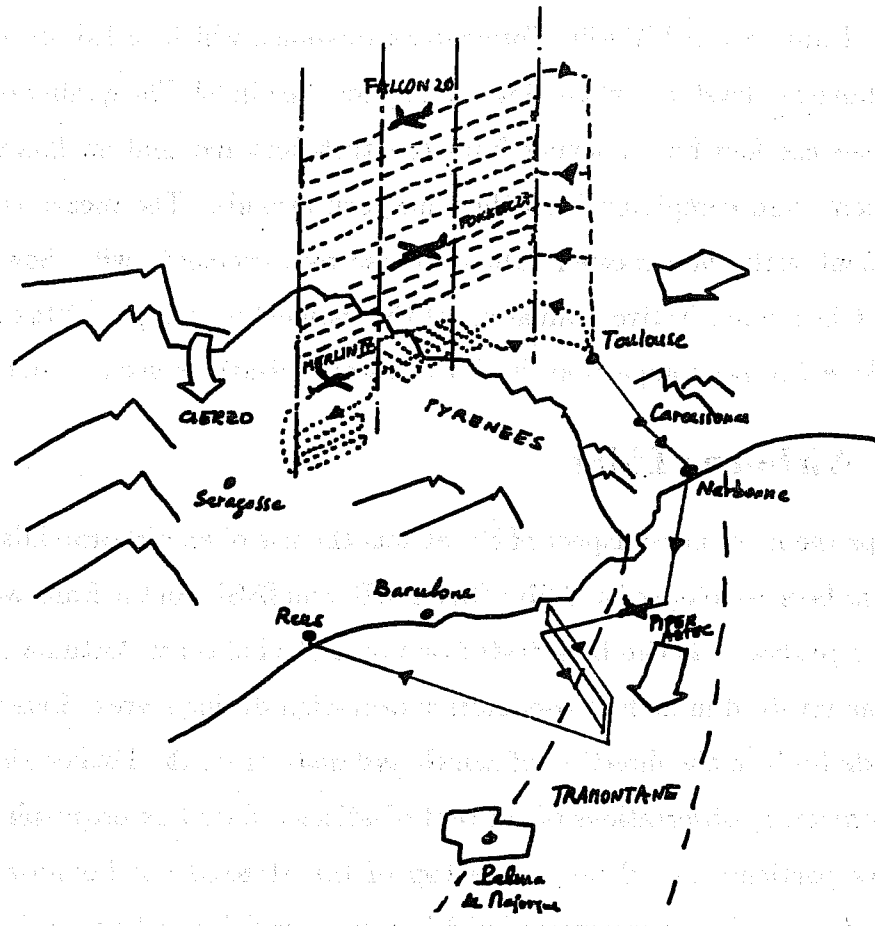

Fig.3: Schematic showing the coordinated flight plans of the Falcon, Fokker, Merlin, and Piper airplanes during a Northern event (IOP 9).

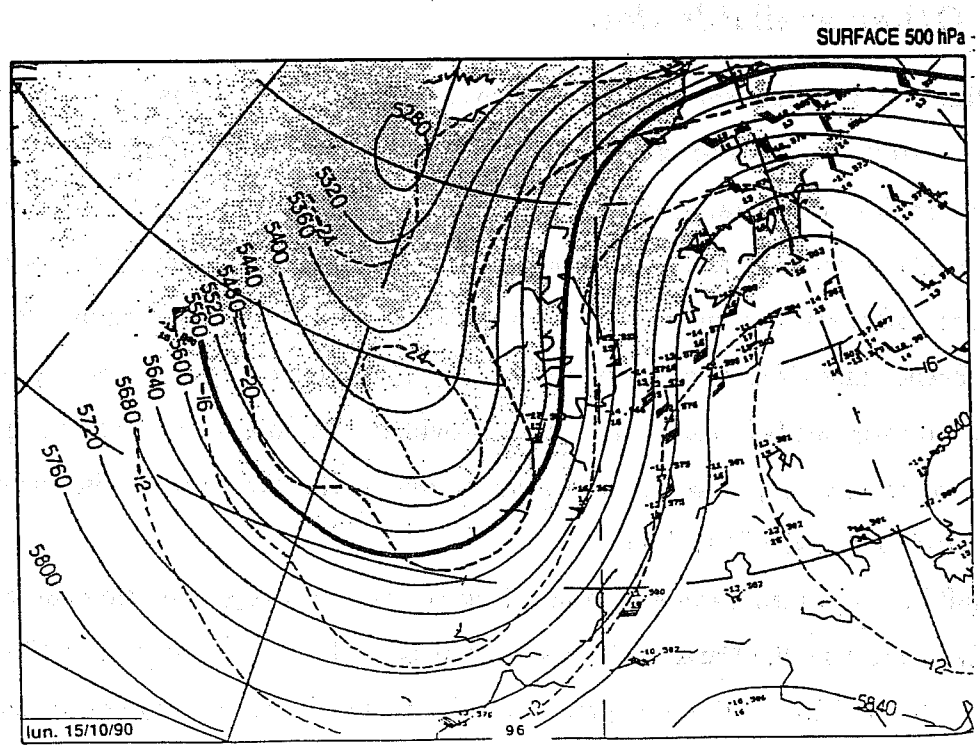

Fig.4: The $500hPa$ chart of 15 October, 1990, 1200GMT.

acquired during the 3 Merlin *Tramontana* missions, which called for about $400km$ flight at $40m$ above sea level, an exhausting exercise for the pilots! The quality of these measurements has been checked by retrieving from the turbulent momentum fluxes an equivalent drag coefficient, and comparing it to the Charnock formula. The measurements showed a good agreement with the expected values. These measurements will allow to take friction into account in a quantitative evaluation of the momentum budget of the accelerated flow, and to make extensive comparisons with the parametrizations used in numerical models.

2.8 Airborne Lidar

Perhaps the most novel aspect of Pyrex was the use of an airborne lidar. A new backscatter lidar has been developed by CNRS (SA, LMD, and INSU) in the framework of the LEANDRE research program. It had been tested on board the Fokker in Autumn 1989 and Spring 1990, and was involved in its first cooperative campaign during Pyrex. Lidar measurements could be made both in the direction of zenith and nadir from the Fokker aircraft. They provided complementary observations of the perturbations induced by orography, as shown by tracers such as particles and clouds. The top of the atmospheric boundary layer is also easily detected by such measurements, and is a very useful quantity for the interpretation of *in situ* measurements. Lidar measurements were performed during nearly all Fokker flights.

2.9 Other available data

In addition to the data-sets discussed above, the Pyrex Data Base contains Météosat and AVHRR visible and infra-red pictures of the area during the IOPs, and the analyses of the meso-scale operational model Péridot of Météo-France (Bougeault and Mercusot, 1992). These products are specifically designed to **initialize** numerical simulations of research models. Some additional measurements are available on a non-systematic basis. At the request of Météo-France and INM, several commercial aircraft companies have made special reports of the wind during the field phase, and have provided these observations to the project group. Data from several ship reports, and some buoys in the Western Mediterranean have also been included into the Data Base.

Finally, a cooperation was established between the project group, the Fédération Française de Vol à Voile and the **French** Airforce authorities. Three civilian and military sailplanes, based in Saint-Girons, (France) participated into the Pyrex operations when the weather permitted, and qualitatively documented the lee wave system. The objective of this operation was to ascertain the 2D nature of the lee wave system, which was thought to be

possible with the qualitative measurements available on-board the sailplanes. In one case, this cooperation resulted in scientifically useful results. But another, more difficult to quantify, benefit of this cooperation, relies in the qualitative appraisal of the Pyrex situations by the sailplanes pilots. Indeed, what we scientists, consider as our best southern case (IOP3), turns out to be a rather common, medium strength situation for the pilots, who had used the Pyrenean lee waves for their fun all year round for many years. This puts in a climatological perspective the conclusions that may be drawn from the Pyrex data on the dynamical impact of the mountain.

2.10 The PYREX Data Base

A significant work has been done, during the last two years, to insure high quality processing of all the measurements. The observations were collected from the various participating groups; they were put in a standard format, and a relational data base system was used to construct an integrated Data Base. This Data Base is running on a dedicated workstation, and is accessible to all participating bodies via the French Research Network. The principal aspects of data organization, access, and quality are discussed by Bougeault and Benoit (1992).

3 An example of strong mountain wave/lee wave system: IOP 3

In this section, we shall try to illustrate the on-going work on one of the best Pyrex situations, the 3rd IOP, that extended from October 14, 1800 GMT to October 15, 1200 GMT, culminating with the aircraft mission, from 0600 to 1000 GMT. The synoptic situation (Fig.4) was dominated by a deep trough extending over the eastern Atlantic Ocean, resulting in a South to Southwesterly flow over Spain and France at all levels above $800hPa$. The whole system was drifting slowly towards the East, and the wind did accelerate steadily during the night, reaching a maximum in the morning of 15th October, just after the aircraft mission. The speed was then about $15m/s$ at $700hPa$, $20m/s$ at $500hPa$, and $40m/s$ at the tropopause, just above $200hPa$. The airmass hitting the range was rather moist, resulting in low-level clouds upstream of the mountain, and alto-stratus formation downstream. It was separated from a dryer airmass to the West by a weak, undulating front, that reached the Western edge of the Pyrenean range at 1200 GMT, 15 October.

The case has been modeled with the research version of the Péridot French Weather

Service operational limited area model. The model is based on the hydrostatic, primitive equation system and has a fairly detailed physical package. It has been validated for similar types of flows by Bougeault(1987), Bougeault and Lacarrère (1989) and Stein(1992). We used a $10km$ horizontal mesh over a domain of 95×95 grid points centered on the Pyrénées, in polar stereographic projection, and a vertical grid of 30 levels regularly spaced by $500m$, with increased resolution in the low levels. This allows to capture the meso-beta scale details of orographic flows. The topography was prepared from the a $1km$ resolution geographic file, and used an envelope orography formulation. It reaches $2900m$, comparable to the averaged height of the main crestline in the central part of the Pyrénées. The model is initialized and forced on the boundaries by the meso-alpha scale analyses interpolated from the grid of the operational model ($35km$ mesh). Note that the assimilation cycle of this model had been rerun with all available upper-air soundings. This procedure ensures that the initial condition of the research model contains no small scale features, and those are created by the model as part of an adjustment to the small scale orography. The run presented here started at 0300 GMT and ended at 1200GMT. The results agree well with the observations concerning the meso-alpha scale patterns (altitude winds away from the mountain, general prediction, etc..), which is not surprising for this very short term forecast, and is entirely due to the good quality of the initial condition. The discussion will therefore focus on the meso-beta scale aspects.

In this fairly typical situation, the Foehn effect started during the night on the northern side of the range, consecutive to the increase in the synoptic wind. The Foehn onset may be seen spectacularly in the temperature and wind time sequences from several stations in the foothills (Fig.5). It follows more or less the eastward drift of the system: The first temperature rise occurs in Biarritz (at the western edge of the range) between 2000 and 2130 GMT. This is followed by several stations in the central part of the range between 2330 and 0030, and the effects propagates to the North between 0100 and 0200. Finally, the eastern part of the range is also reached by the Foehn effect between 0400 and 0500. This is accompanied nearly everywhere by drying and increased southerly wind. The maximum wind gust observed is $16m/s$, from South, in Lannemezan (Central Pyrénées). At sunrise time on October 15th, the temperatures reached 18°C in all of south-west France, and more than 20°C in the foothills, an unusually high value for the season.

During the aircraft mission (morning of 15th), there was not much change in this situation. A general view of the surface wind at 0800GMT (Fig.6a) shows that the Pyrex area is divided in several well-identified subdomains. The northern foothills are under the influence

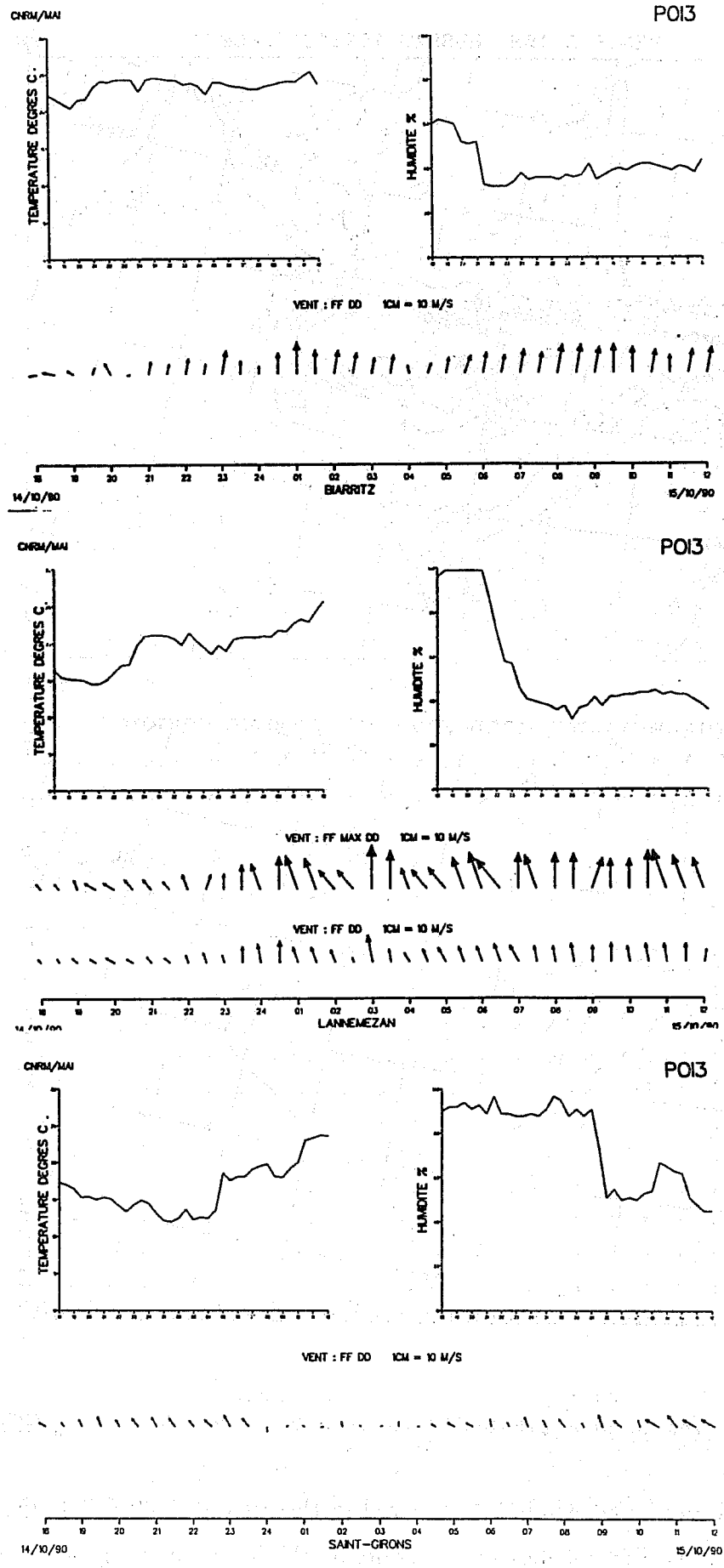

Fig.5: Time sequences of winds and temperatures at some stations of the Pyrenean foothills, showing the Foehn onset during the night from 14 to 15 October, 1990.(from Champeaux and Péris, 1991).

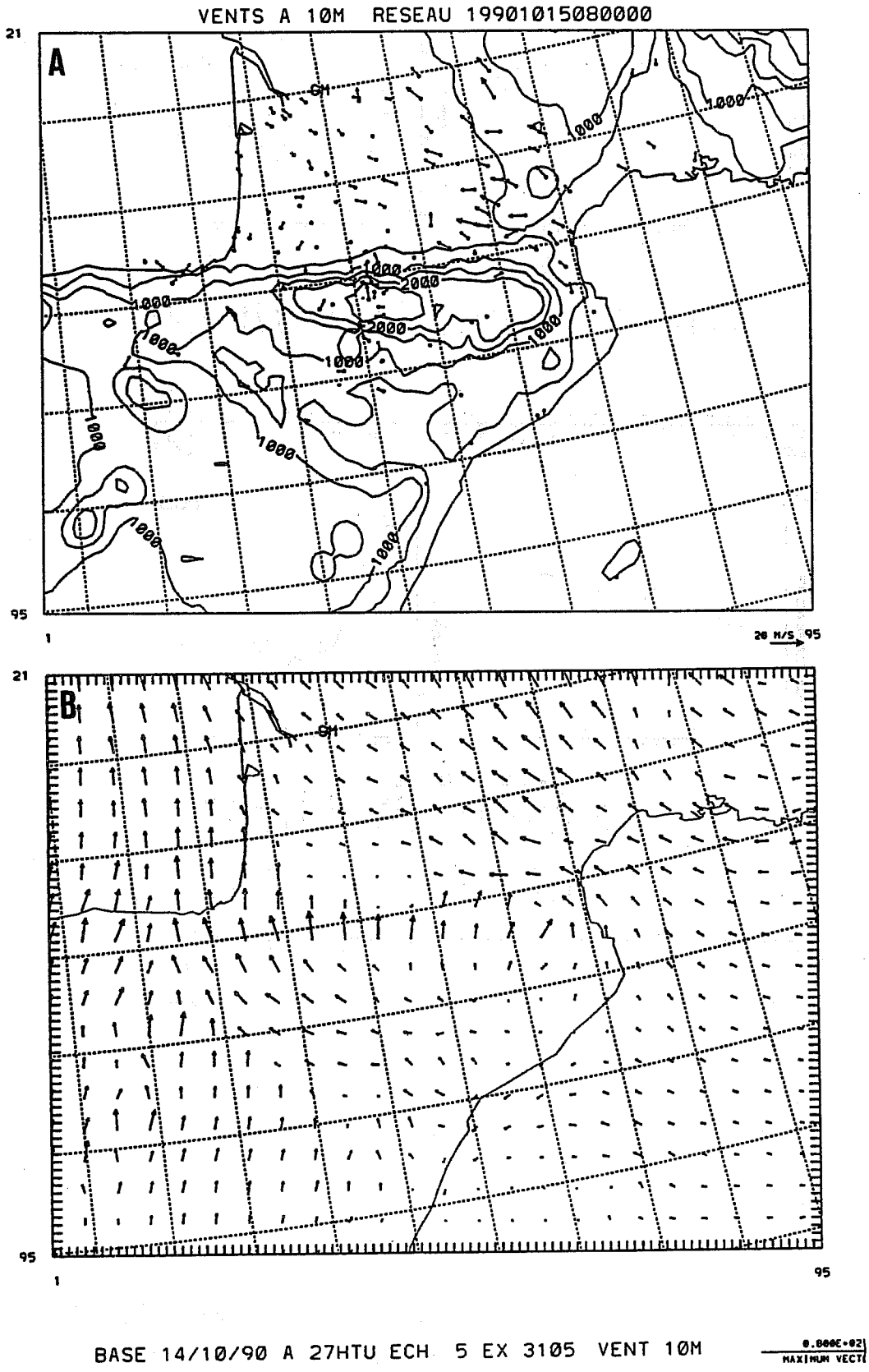

Fig.6: Surface ($10m$ level) winds (a) observed in the area at 0800 GMT, October 15; (b) simulated by the Péridot meso-scale model of Météo-France (only one vector evry fourth grid point is shown).

of the Foehn, with southerly winds reaching $10m/s$ in the central part. Going to the North, we find an area of weak and disorganized winds, which corresponds well with the climatological wind speed minimum in this area, due to the sheltering effect of the range. Moving to the East, one enters the domain of the *Autan* wind, that starts as usual upstream of the Naurouze path, accelerates between the slopes of Pyrénées and Massif Central, and extends until the Gers hills to the West. The maximum intensity is seen to occur on the southern slopes of the Massif central, and reach $15m/s$, with $20m/s$ instantaneous gusts reported. This is confirmed by the Baraignes Sodar, which measured $15m/s$ surface wind, increasing to $25m/s$ at $400m$ above ground. It will be interesting to study which part of the wind is caused by the Pyrénées alone, and which part is due to the channelling between the two mountain ranges. Further to the West, southerly winds in agreement with the upper level flow are observed. Finally, on the upstream side, the flow is clearly channelled into the Ebro valley, leading to a southeasterly wind directed towards the western edge of the Pyrénées. That feature may explain why the Foehn is in general stronger on the western side of the Pyrénées and on the near-by Basques mountains. The surface wind predicted by the model at 0800 GMT is shown in Fig.6b, and may be directly compared with the observations in Fig.6a. The different areas identified in the previous discussion are well reproduced. The main problem seems to be the underestimation of the maximum speed of the *Autan* wind by the model.

On that day, the Piper aircraft performed one of its 6 *Autan* flights. The flight plan called for oblique soundings between Toulouse and the mediterranean coast, to document the depth of the shallow wind layer. These measurements have been processed, together with the near-by soundings, to produce the synthetic wind and temperature cross-sections shown in Fig.7a,b. They depict a $20m/s$ easterly wind, extending from the surface to $1000m$ a.s.l., capped by a strong temperature inversion. Note that the inversion is not present in the upstream part, meaning probably that it is generated by dynamical processes forced by the orography. The second part of the flight plan called for a track at $935hPa$ (the level of wind maximum), documenting the horizontal structure of the flow (Fig.8a). This track clearly shows a progressive wind rotation from the South-East on the eastern side of the range, to due South in the central part. The maximum wind speed measured by the Piper exceeds $22m/s$ (in agreement with the surface and sodar measurements) and is located nearly above Toulouse. The simulated vertical cross-section (Fig.7c,d) confirms that the model slightly underestimates the maximum wind speed. It also underestimates the strength of the inversion, perhaps because of unsufficient vertical resolution. According to

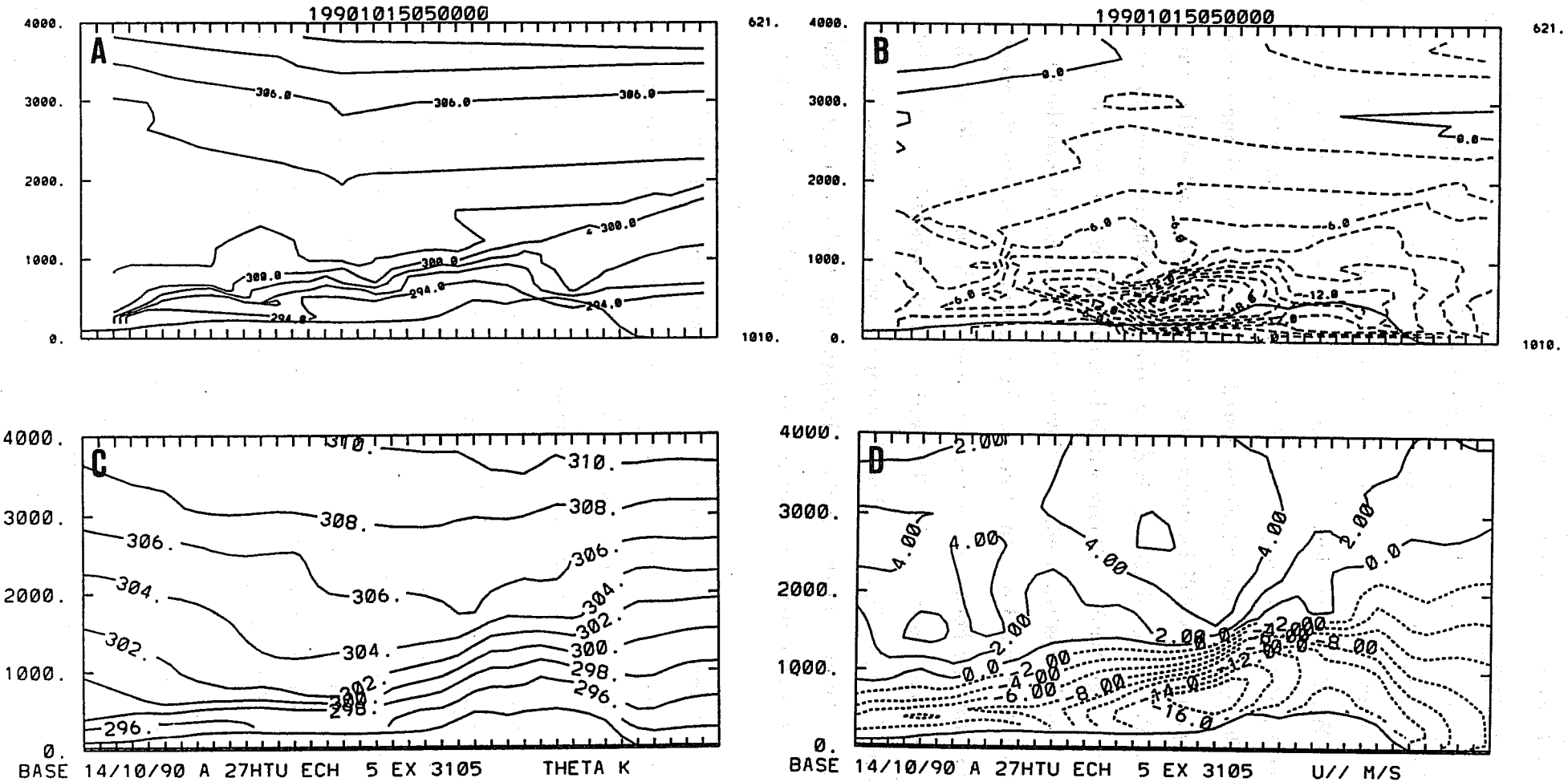

Fig.7: Vertical cross-sections along the *Autan* wind principal axis (see the position of the cross-section on Fig.8). (a) Potential temperature interpolated from measurements of soundings in Port La Nouvelle, Toulouse, and Pau, and of the Piper flight.(b) Wind component parallel to the cross-section, interpolated from the same data sources. (c) Potential temperature simulated by the Péridot model. (d) Wind simulated by the Péridot model.

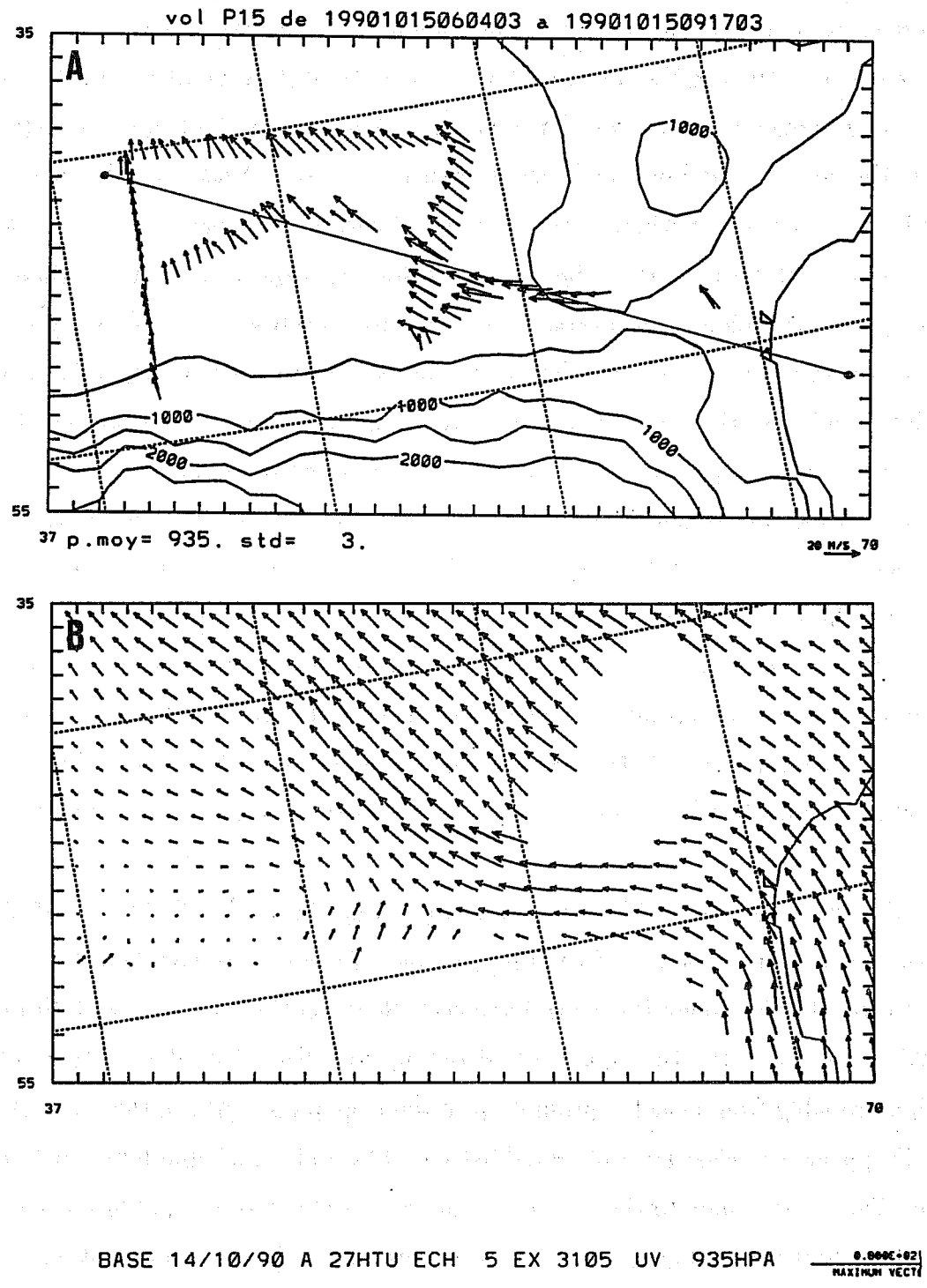

Fig.8: Horizontal cross-sections of wind at $935hPa$ in the *Autan* domain. (a) Observations of the Piper flight (the axis of the vertical cross-section in Fig.7 is shown as a thin line). (b) Simulation of the Péridot model.

the hydraulic theory for torrential flows, these two problems are connected, and further experiments will be conducted with increased vertical resolution. The simulated $935hPa$ cross-section is shown in Fig.8b. The model reproduces well the horizontal extend of the *Autan*, but underestimates the southern flow in the wake of the central part of the mountain.

To study the main mountain wave, the Falcon, Fokker and Merlin flights above the central transect, the nearby soundings, and the observations of the CNRM portable network have been used to construct synthetic cross-sections of several parameters. The method used is fairly simple. It assumes that the flow is stationary, projects the data orthogonally to the selected vertical plane, and averages them to the spatial scales resolved by the model, i.e. approximately $10km \times 500m$. Thus, lee waves are filtered (see below for a lee wave discussion), and only the main mountain wave remains. Since the synoptic wind was still slightly increasing during that period, the effects of "unstationarity" will need a careful study in forthcoming work. The potential temperature cross-section obtained by this method (Fig.9a) nevertheless shows a well established mountain wave, extending up to the lower stratosphere, with a slow phase reversal in the troposphere, and a weak, but definite, upstream tilt. One may therefore expect a negative associated momentum flux, as shown below. Note that the less pronounced wave amplitude at $7000m$ a.s.l may be due to the absence of data at this height. This mountain wave is fairly well simulated by the model, as shown by the vertical cross-section in Fig.9b, to be compared to Fig.9a. On this picture, the Foehn effect is also obvious.

The airborne LEANDRE lidar was operating during the Fokker flights of IOP 3. Fig.10 shows the vertical cross-section of the range corrected signal obtained from the surface up to an altitude of $10km$ along the central transect. South of the Pyrénées, at latitudes lower than 42.5N, the cloud structure appears horizontally stratified with different types of clouds, extending probably from near the ground up to the tropopause. Above the crest, the clouds totally disappear, and clear air is observed between 42.6 and 42.8N, and between 4 and 12km altitude. This corresponds to the subsidence noted in the composite potential temperature cross-section discussed at Fig.9, and confirms the structure of the main mountain wave. The altostratus then reappears and seems thicker than upstream, as confirmed by the available satellite images. In the low levels (near $4000m$), small clouds are seen at the top of the lee-waves. They look similar to the clouds seen on the satellite image some hours later.

Indeed, as usual in such case, lee-waves were excited downstream of the range. These waves were topped by cloud bands, and visible from the ground during most of the day. They can be seen on the NOAA11 AVHRR 1417 GMT visible image in Fig.11. It is unfortunate

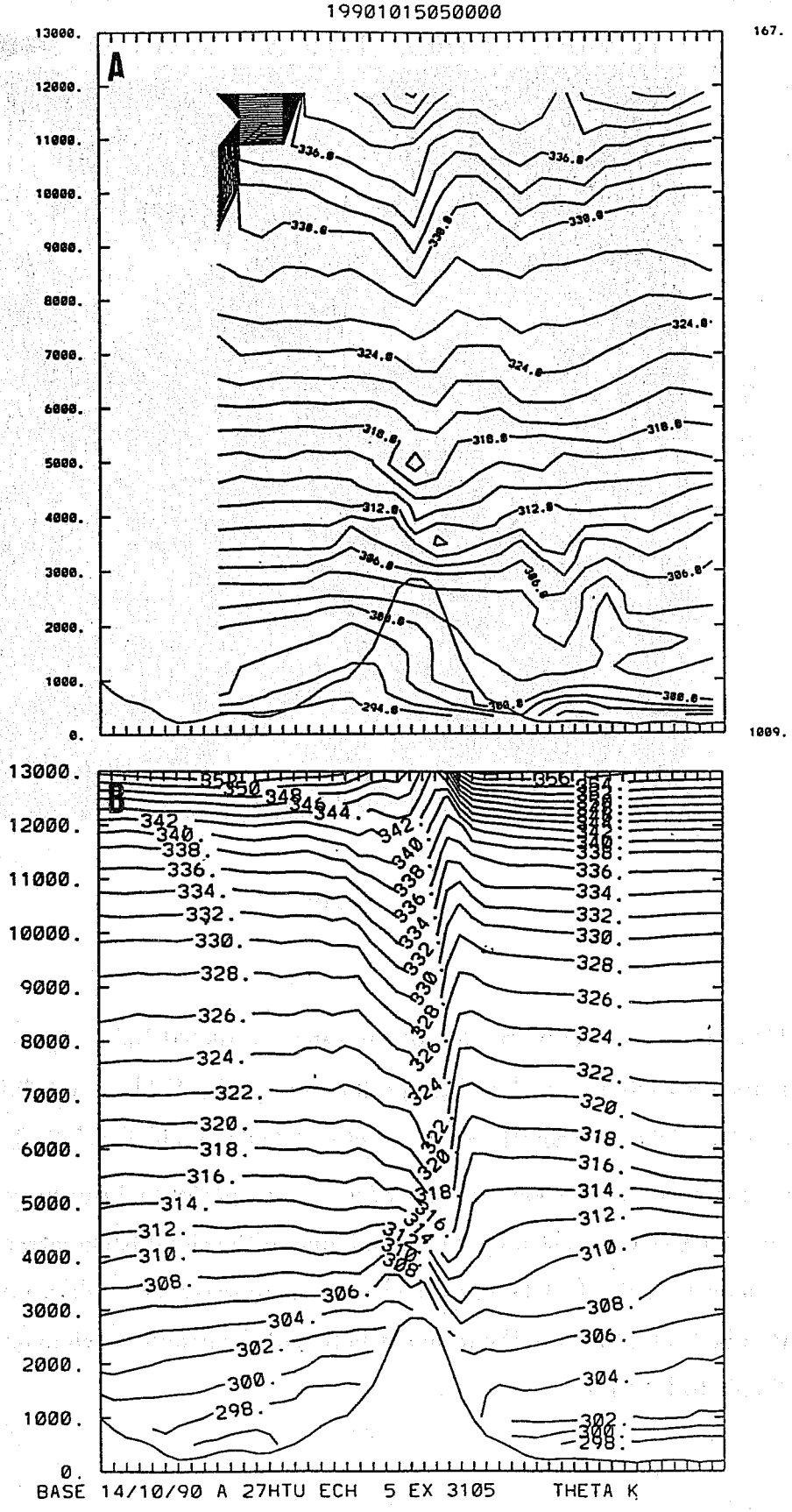

Fig.9: Vertical cross-sections of the potential temperature along the Central Transect: (a) obtained by interpolation of measurements of the Fokker, Falcon, and Merlin flights, of radiosondes, and of the measurements of the CNRM portable network; (b) Vertical cross-section of potential temperature simulated by the Péridot model.

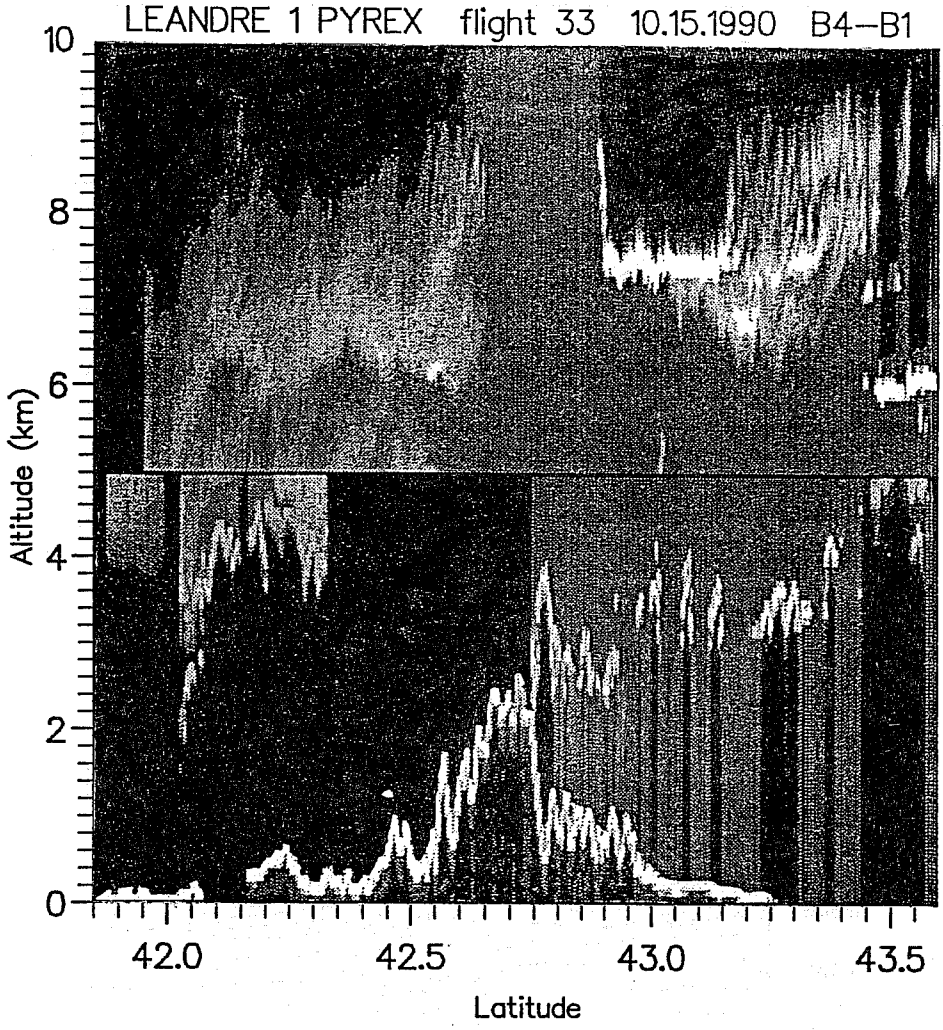

Fig.10: Central transect cross-section of the range corrected Lidar signal. This image has been reconstructed from two legs performed by the Fokker at $5700m$ for nadir viewing, and at $4700m$ for zenith viewing, between 0602 and 0727 GMT. The mountain shape is reproduced from clear-air lidar observations performed during another flight. Cloudy areas are characterized by high signal due to the cloud backscatter, reported on the figure as whiter pixels, whereas the clear air is represented as dark pixels, however some dark pixels also indicate the total extinction of the beam, which makes the picture more difficult to interpret.

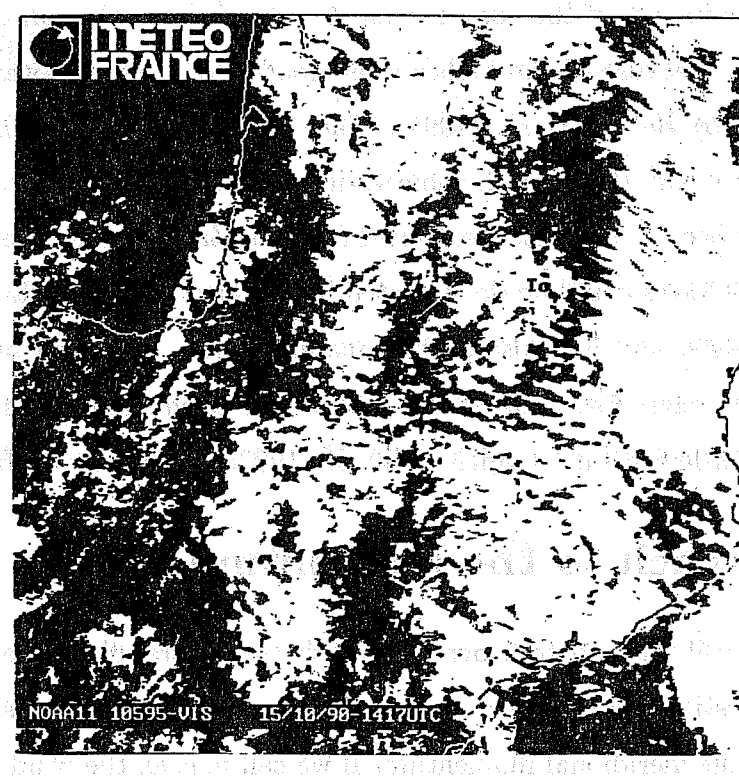

Fig.11: Picture obtained from NOAA11 visible channel on 15 October, 1417GMT

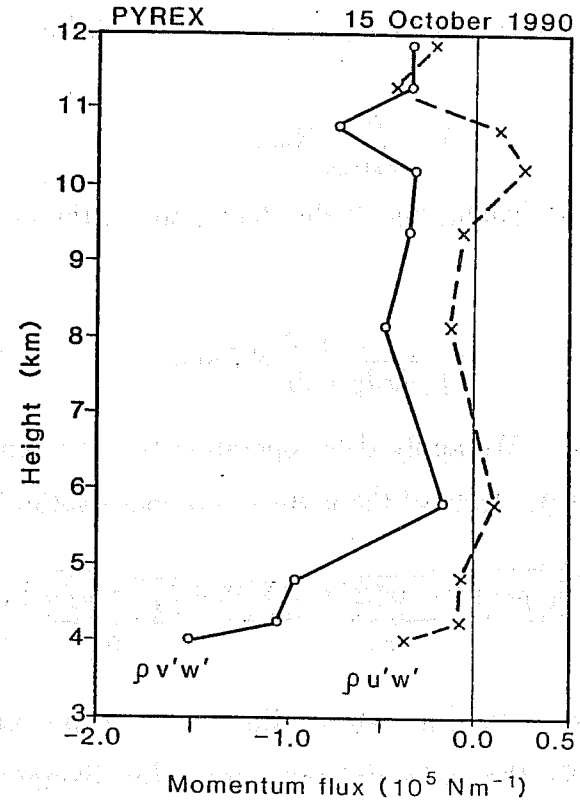

Fig.12: Wave momentum fluxes computed from the Fokker and Falcon flights above the Central Transect (courtesy of K.P. Hoinka).

that earlier satellite images of that day cannot give any information on the lee-wave during the aircraft mission, because of the higher level cloud cover. The lee-waves event of IOP 3 has been described by Bénech et al. (1991). They showed that the horizontal wave-length of these waves was about $10km$, with some variations with the altitude, and found a good agreement with the Scorer parameter computed from the Zaragoza (upstream) sounding from 0600 GMT. The lee waves could be documented by the aircraft, the balloons, the sailplanes, the lidar, the profilers, and had also surface manifestation, as shown by the Lannemezan sodar data. The lee waves observed during IOP 3 have been simulated numerically by two two-dimensional non-hydrostatic models (Elkhalfi, 1992; Satomura and Bougeault, 1992).

4 An approach to the momentum budget

In this section, we will attempt to progress towards the central objective of the experiment by **summarising** existing informations on the momentum budget for this case. For brevity, we concentrate on the meridional momentum. If we call u, v, w, the wind components, ρ the air density, p the pressure, and f the Coriolis parameter, the meridional momentum equation reads:

$$\partial_t(\rho v) + \partial_x(\rho uv) + \partial_y(\rho v^2) + \partial_z(\rho vw) + \partial_y p + \rho f u = 0$$

To volume average this budget in three-dimensional boxes, we define a vertical integration operator

$$\tilde{A} = \int_{h(x,y)}^{Z} A dz,$$

where $h(x,y)$ is the local terrain height, and Z the (fixed) top of the integration box; and a horizontal averaging operator

$$\bar{A} = \frac{1}{\int\int_D dxdy} \int\int_D A dxdy,$$

where D is a horizontal domain. We apply these operators to the momentum equation, to obtain the Euler theorem (integral form of the momentum conservation)

$$\underbrace{\partial_t(\overline{\tilde{\rho}\tilde{v}})}_{E} + \underbrace{\overline{\partial_x(\rho\tilde{u}v)} + \overline{\partial_y(\tilde{\rho}\tilde{v}^2)}}_{C} + \underbrace{\overline{\rho v w(Z)}}_{B} - \underbrace{\overline{\rho_s v_s w_s}}_{G} + \underbrace{\overline{\partial_y \tilde{p}} + \overline{\rho \tilde{f} u}}_{H} + \underbrace{\overline{p_s \frac{\partial h}{\partial y}}}_{F} = 0 \qquad (1)$$

where the different terms are in Pa (momentum flux, or force per unit surface). They represent the time evolution (E), the horizontal momentum flux divergence (C), the vertical flux of momentum (B), the surface turbulent friction (G), the ageostrophic force (H), and the surface pressure drag (F). As explained in the introduction, some of these terms are

accessible by measurements, for certain areas. For instance, if we choose the y axis parallel to the central transect, the surface pressure drag is available from the CNRM portable network measurements (see Section 2.2). Also, the wave momentum fluxes above the central transect can be computed from the meridional and vertical velocities measured by the Fokker and Falcon airplanes, although this kind of computation usually involves a lot of uncertainties. To minimize these uncertainties, we removed the mean and trend, using a quadratic regression, and suppressed small-scale waves (smaller than $5km$) with a low-pass filter. The results are shown in Table 4 and Fig.12. The surface pressure drag is about $6Pa$, whereas the wave momentum flux decreases from $-0.8Pa$ in the lower troposphere to $-0.2Pa$ between 6 and $10km$, and has a secondary maximum of $-0.4Pa$ at $11km$. Thus, the wave momentum flux is only a small fraction of the surface pressure drag, in agreement with the findings of Hoinka and Clark(1991) over the Alps.

The other terms of the budget must be deduced from model results. We have developed a diagnostic computation of these terms using the results of the Péridot model of Météo-France (Stein, 1989). For any desired box, consisting of a rectangular subdomain of the computation grid, the terms of Eq.2 are computed for all heights Z above the highest topography present in this subdomain, and a residual is computed to assess the validity of this off-line computation. The residual is usually found very small. These computations have been performed by Beau(1992) on the simulation discussed above in Section 3, for two different boxes shown in Fig.13. The smaller box is called the *validation box.* It is designed to provide a computation as comparable as possible to the Central Transect measurements. Results for this box are shown in Fig.14a. Note that all values represent quantities integrated from the surface to the level given in ordinate, not local quantities. The surface terms (pressure and frictional drag) are therefore constant with height, and the vertical flux of momentum (B) has its usual meaning. These results must be compared to the observed values of Table 4 and Fig.12. The model reproduces very well the surface pressure drag of about $6Pa$, but it overestimates the wave momentum flux in the low levels by a factor of 3. It correctly reproduces the decrease in altitude of this flux, reaching very small values between 6 and $9km$, and increasing again above $9km$. It is very encouraging that the model wave momentum flux is so similar to the observed one. Also, it is interesting that the model predicts a variation of the wave momentum flux with altitude, although there is no wave breaking in this case, and the dissipation of wave energy by turbulence remains very small. This illustrates how much the 3D dynamics of these phenomena differ from the conventional 2D dynamics. In the present case, the budget is closed by the ageostrophic pressure force and the horizontal momentum

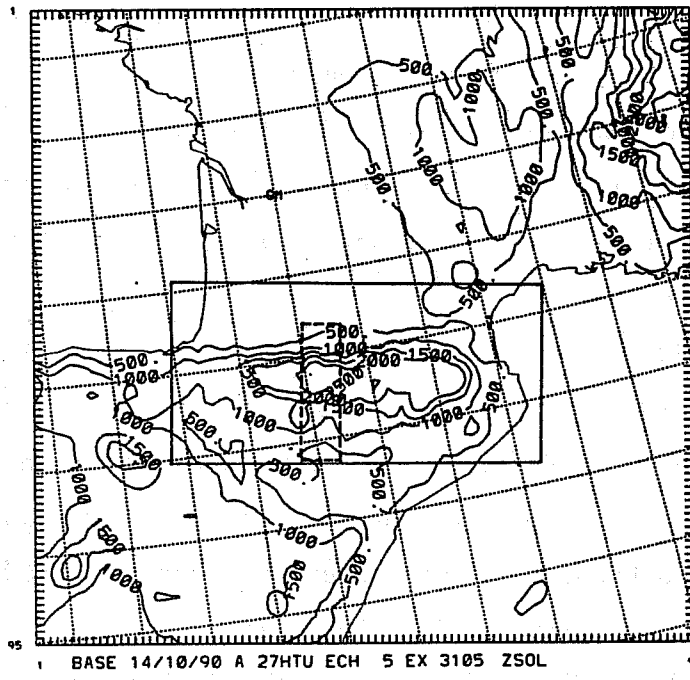

Fig.13: Horizontal domains for the momentum budget computations with the outputs of the Péridot model. The smaller box is the *validation box* covering only the Central Transect. The larger box is well fitted to an evaluation of the global effect of the mountain.

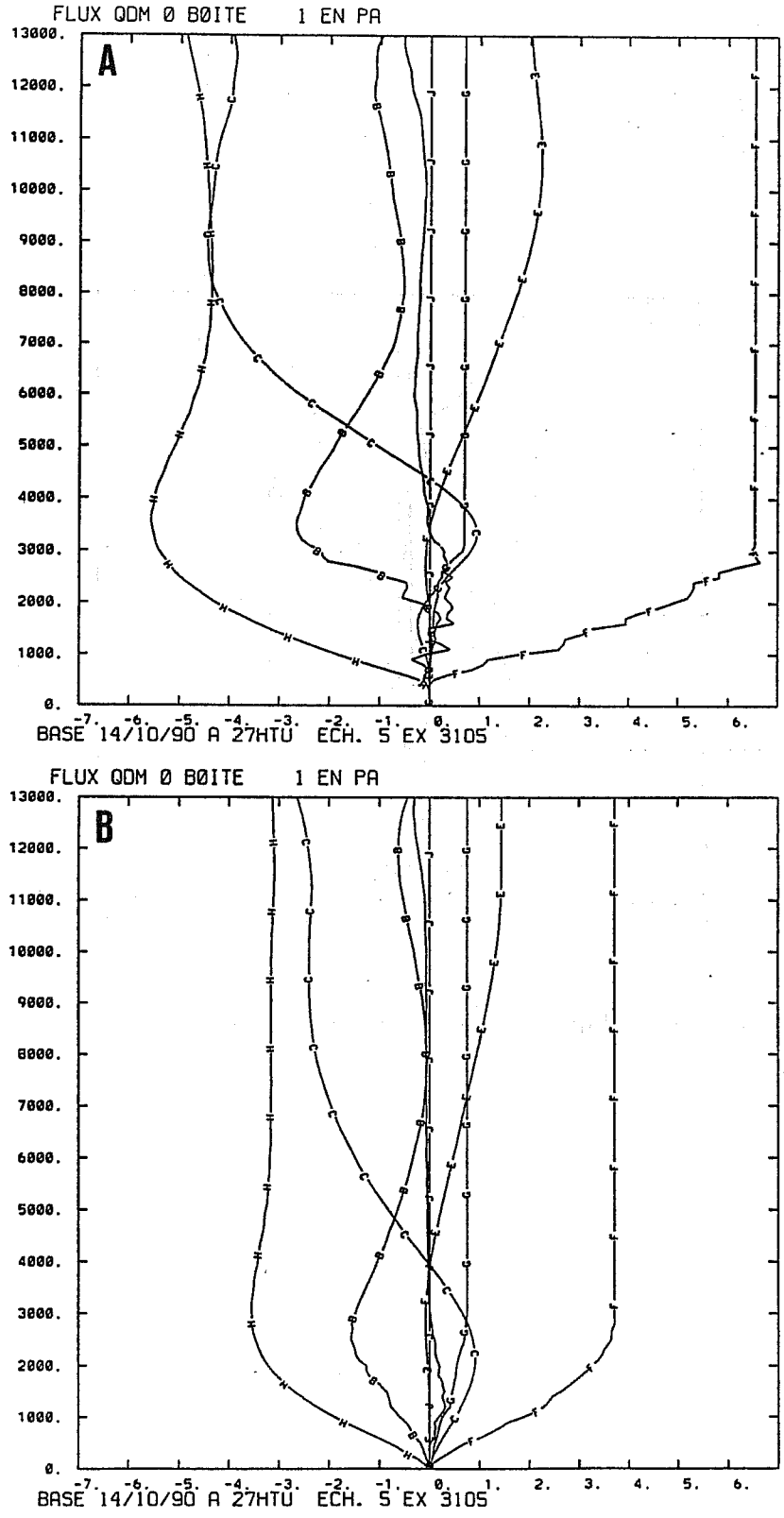

Fig.14:(a) Momentum budget computed in the *validation box* from the outputs of the model (see text); (b) Same as (a), but on the larger box. The letters refer to the terms of the budget discussed in the main text.

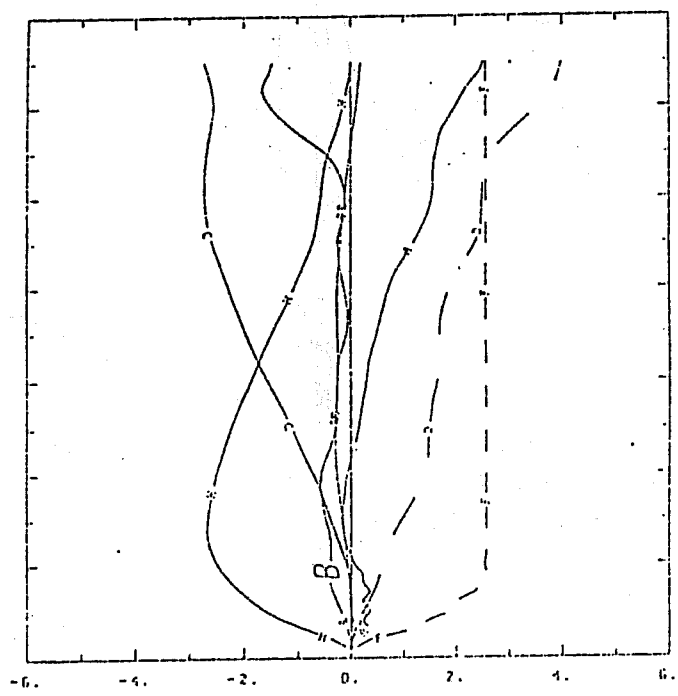

Fig.15: Same as Fig.14, but obtained by interpolation of available soundings (from Benoit, 1992).

advection, and the situation is clearly not stationary in the higher levels. This means that the real problem is not to understand why the wave momentum flux differ from the surface pressure drag in observations, but to understand whether the model must still be improved to get quantitative agreement with observations of the wave momentum flux (without changing the value of the pressure drag!), or if we accept that observations underestimate the observed momentum flux in the lower levels (there are a number of difficulties in the determination of the vertical velocity from aircraft that could explain this).

Next, the budget has been computed at the scale of the entire range, using the larger box of Fig. 13. The results, on Fig.14b, are very similar to those of the smaller box, but scaled down.

An independent determination of the momentum budget has been made by Benoit (1992), from data interpolated from the 11 soundings only. He made a two-dimensional univariate analysis of pressure, density, altitude, and wind vectors, using a vector spline technique along sigma levels, over the same horizontal domain as in our numerical model. He then used the same diagnostic computation of the different budget terms. His result is shown in Fig. 15. For the lower levels, it is very comparable to the model-derived budget (Fig.14b). It is very encouraging to find that the shape of the wave momentum flux is again very close to the aircraft determination of Fig.23 (the values themselves cannot be compared, since this is a much larger box). The surface pressure drag is nearly the same as in the model large box case, but the low level wave momentum flux is about half that of the model, which would tend to confirm that the model value is too large . The agreement is not so good in the upper levels, mainly because of the ageostrophic force and time variation terms. This results in a strong residual term, indicating that the budget is not closed in the upper atmosphere. Present work is directed at understanding this problem. Nevertheless, it is clear that this kind of model/data comparison will be a very efficient source of progress in the near future.

5 A preliminary assessment of the accuracy of GWD parametrizations

For this section, we temporarily admit that the model results are good enough to represent the reality, and we give an illustration of the type of exploitation that can be made from such results. The focus is on the verification of the parametrizations of mountain wave drag, one of the primary objectives of PYREX. Our model-derived momentum budget (Fig.14) is considered as the truth, and we want to deduce from this budget the "small-scale part" that

a parametrization should represent in a larger-scale model. The problems to address are the followings:

- What is the size of the box that should be considered to make these computations?
- What kind of large-scale profiles should be entered in a parametrization under study?
- What part of the budget should the parametrization deliver as an ouput?

We do not pretend that our answers to these questions are the best possible, at the present time they are mostly working hypotheses.

The most natural answer to question 1 seems to be the size of the large-scale model grid. However, present day "large-scale models" have grid sizes smaller than $100km$. This enables them to resolve part of the orography of, e.g., the Pyrenean range. It appears difficult and unphysical to split the effect on the momentum budget of the mountain wave shown in Fig. 9 into components associated to every single grid point of a large-scale model. Furthermore, parametrizations are not expected to deliver an output valid at the grid-point scale, but they should be evaluated on domains of a few grid points. Therefore, we decided for the time being to work with boxes having roughly the size of the entire mountain range. This means that we try to reconstitute the budget shown in Fig. 14b by a large-scale model plus a GWD parametrization working at the scale of the large box of Fig.13. The input of the parametrization are profiles averaged over this box, and the outputs should be viewed as desirable averages over the same domain. This provides an answer to question 2. Coming now to question 3, it is clear that only this part of the budget, which is not resolved by the large-scale model, should be delivered by the parametrization. Otherwise, certain terms would be double counted. The approach we have taken to find this contribution is to run a version of the Péridot model having the same characteristics than the reference run discussed above, but with the topography smoothed to the resolution of a "large-scale model". The results of this run are viewed as an approximation of what a "large-scale model" would simulate over the same area. Of course, this is only an approximation, since a real large-scale model would suffer from different numerical errors than does our smoothed model. However, the results are enlightening.

Two examples of the differences between the full resolution and smoothed orography experiments are shown in Fig.16. Despite the model conserving a basic resolution of $10km$, it is clear that the results of the second run are very smooth. It is therefore reasonable to average horizontally the results of this run, in order to provide input profiles to the

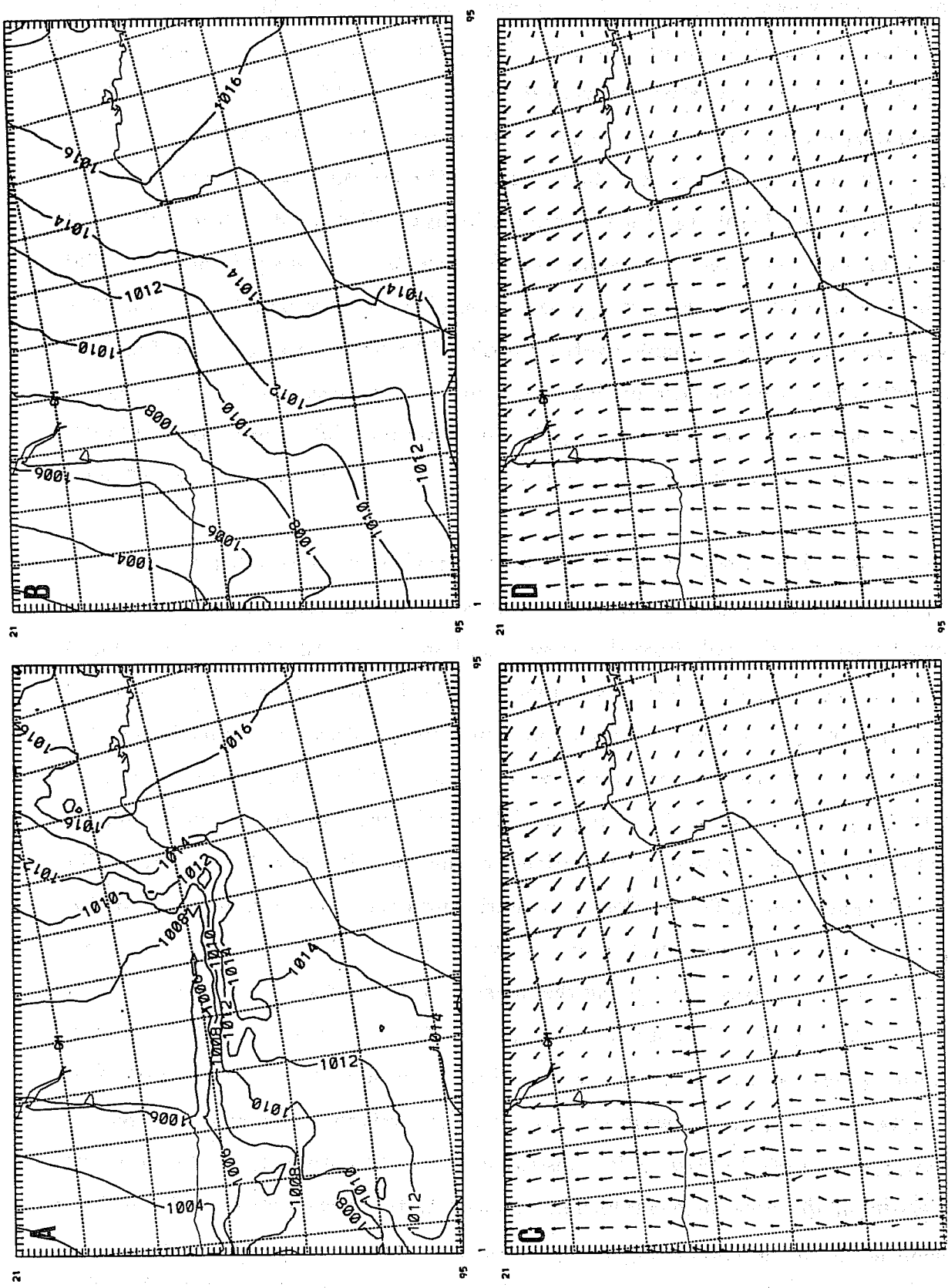

Fig.16: Examples of the differences between the reference and smoothed runs: (a) Sea level pressure in the reference run; (b) Sea level pressure in the smoothed run; (c) Surface winds in the reference run; (d) Surface winds in the smoothed run.

parametrization. On the other hand, the momentum budget resolved by the smoothed orography run is shown in Fig. 17. It is in many respects comparable to the reference budget of the full resolution run (Fig.14b). This shows that, as far as the momentum budget is concerned, the smoothed run already captures a significant part of the process, and the parametrization has just to supply a minor part. This "parametrizable part" is obtained by substracting term by term the budgets of the two runs, and the result is shown in Fig. 18. It is remarkable that in this residual budget, all terms have canceled except the surface pressure drag, the wave momentum flux, and the ageostrophic pressure. This means that the presently widely used approach, consisting in **parametrizing** the effects of unresolved mountain waves by purely vertical transfer (the surface pressure drag F and the vertical profile of the wave momentum flux B) can obtain some success, if it delivers outputs in agreement with the values shown in Fig.18, and *if the model dynamics adjusts itself in response to the parametrization in such a way as to simulate the change in the ageostrophic term H.*

We have tested in this way two different parametrizations corresponding to the formulations presently operational at ECMWF and Météo-France (Beau, 1992). In both cases, we obtained a copy of the code from the operational libraries, in order to avoid introducing interpretation errors. Input profiles were computed as horizontal averages on the large box of the prediction of the smoothed orography run (wind, temperature, and humidity profiles). The subgrid-scale variance of the orography, which is the most important ingredient of these parametrizations, was computed by taking the difference between the full resolution and the smoothed orography and computing the variance of this quantity over the same box. This resulted in a value close to $600m$. Both parametrizations then *underestimated* the surface pressure drag and the wave momentum flux shown in Fig.18. Next, we allowed for some tuning of the numerical coefficient giving the intensity of the surface pressure drag. In the Météo-France formulation, the optimal calibration of this coefficient resulted in a tenfold increase with respect to the operational value. With this modification, the direction of the pressure drag predicted by the parametrization matched well the value required from the residual budget (note that this direction was not used for the optimization). However, the vertical profile of the wave momentum flux supplied by the parametrization did not decrease sufficiently in the lower levels to reproduce the difference observed in our residual budget between the surface pressure drag and the wave momentum flux. In the ECMWF parametrization, on the other hand, the optimization resulted in a four times increase of the coefficient. With this optimal value, the direction of the surface pressure drag was less well

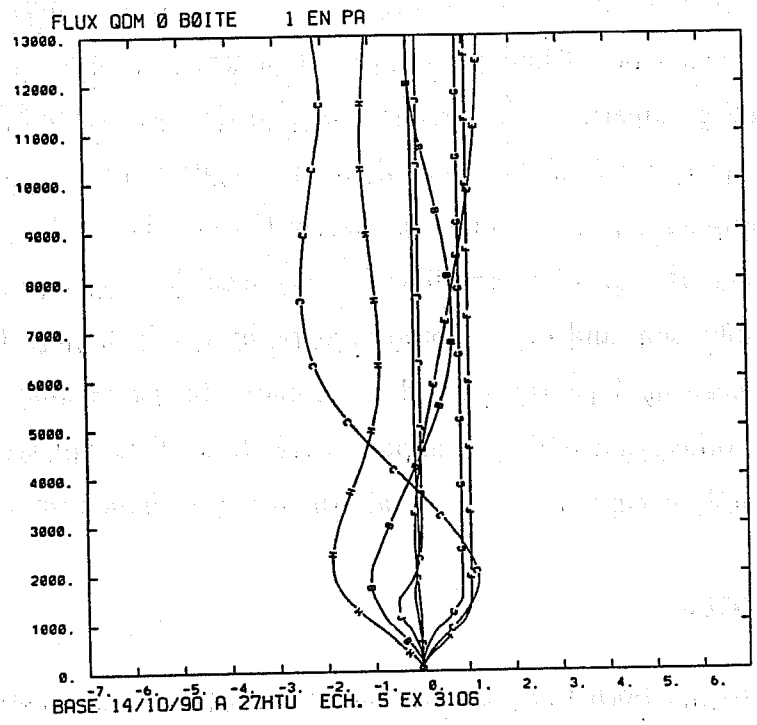

Fig.17: As in Fig.14b, but with outputs of the smoothed run.

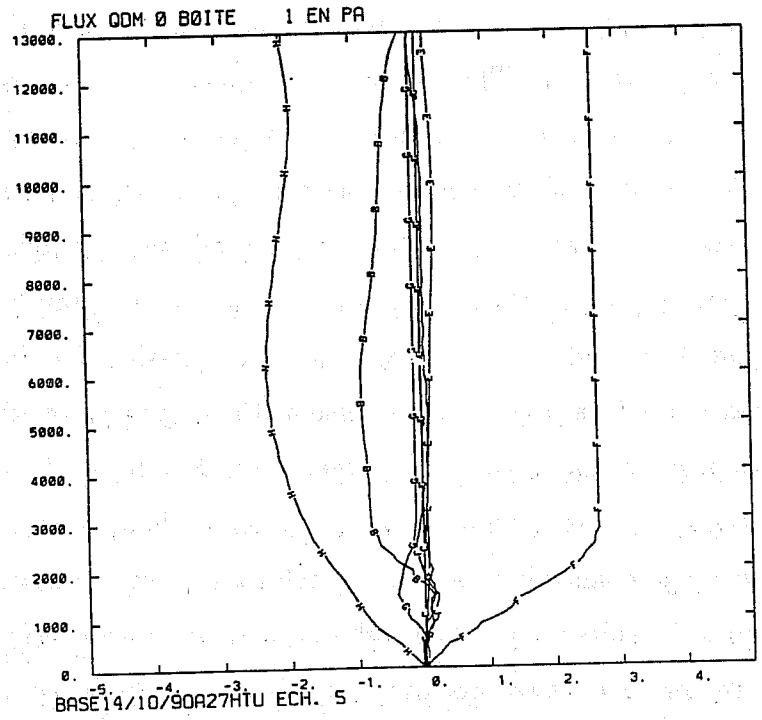

Fig.18: Term by term difference of the momentum budgets of the reference and smoothed runs.

predicted than in the previous case, but the low level wave momentum flux matched closely the value required by the residual budget (Fig.19). This was considered an interesting result, and the ECMWF parametrization was introduced in the meso-scale Péridot model for an on-line test, in order to verify if the model dynamics would indeed supply the expected adjustment of the ageostrophic term. This was nearly the case in our first short ($6hours$) simulation: Fig 20 shows the term by term difference between the momentum budgets of the full resolution orography run, and the smoothed orography run including the parametrization: All terms have been significantly reduced as compared to the residual budget between the reference and smoothed runs without the parametrization. This indicates some success. Further work is presently beeing done to ascertain the value of these preliminary findings.

6 Conclusions

We have tried to illustrate both the diversity and the quality of the measurements made during PYREX, and the general strategy of the scientific exploitation. The phenomenology documented by PYREX data is not new, but the complementarity of the observation means, and the systematic use of numerical models, open the way to an accurate evaluation of higher order quantities, like the terms of the momentum budget. Several questions remain to be solved concerning the measurements, whereas intercomparisons between data sources allow to assess their value more precisely. There is place for much more detailed studies of each data-sets, relaxing the time and space resolution constraints imposed by our comparison with meso-scale models. Only such focused investigations can help to build the confidence in the various data-sets, and to assess the values of our preliminary conclusions concerning the momentum budget. Several of these studies are already in progress (e.g. Attié et al., 1992; Tannhauser and Attié, 1992). Others will be made possible by the decision of the project group to release the data base for public use at the beginning of 1993.

So far, the computation of the momentum budget in the Péridot model of Météo-France, has allowed interesting comparisons with the measurements. Work remains to be done to understand the present discrepancy between the modeled and observed fluxes of momentum, and to decide if the model results are good enough to constitute a firm basis for parametrization validation, but the present results are encouraging. Our preliminary determinations of the parametrizable part of the momentum budget supports the idea that unresolved mountain waves can be represented in large-scale models by a purely vertical momentum transfer. They show some success for present versions of existing operational parametrizations, al-

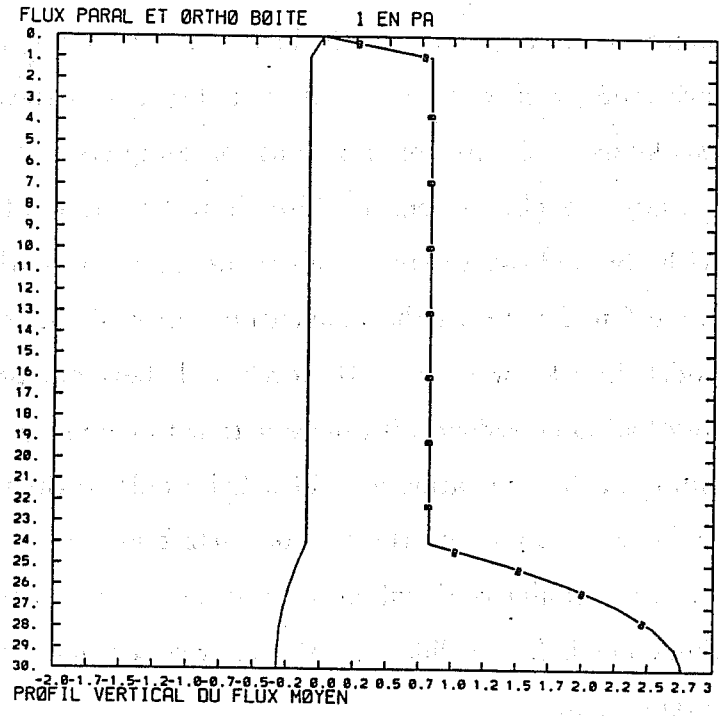

Fig.19: Wave momentum flux predicted by the ECMWF parametrization of moutain wave drag, using a numerical coefficient increased by a factor of 4. (meridional component of the wind)

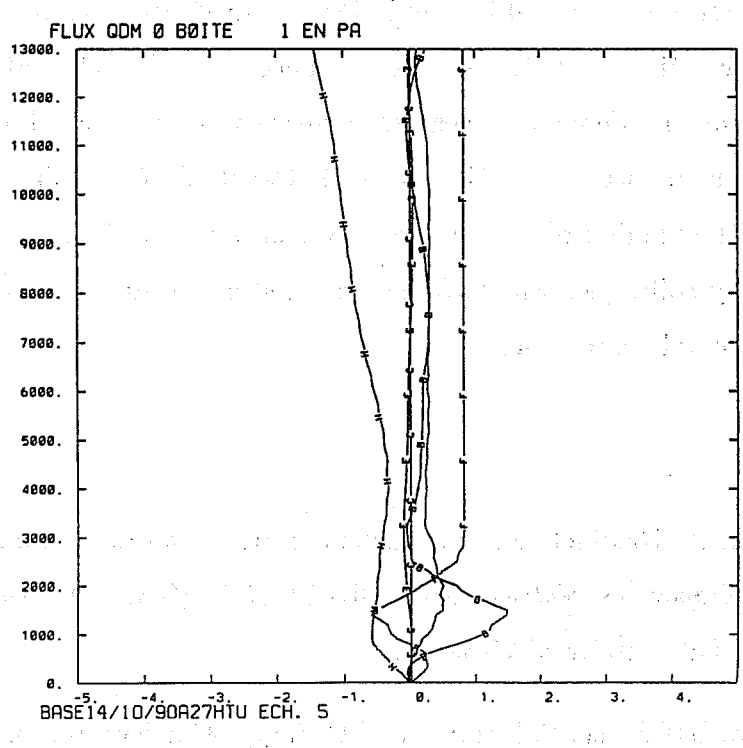

Fig.20: As in Fig 18, but for the difference between the reference run and the smoothed run including the parametrization. The terms have been significantly reduced as compared to Fig.18.

though the optimal values of the adjustable coefficients differ significantly from the ones presently adopted. Much more work will be needed to understand if these differences correspond to an actual weakness of the parametrizations, or compensate for other problems not considered in this study (roughness, etc..). Also, it will be interesting to reproduce similar computations with non-hydrostatic small scale models, since recently (Durran, 1991) important differences were found between the momentum fluxes simulated by hydrostatic and non-hydrostatic models in a lee-wave case. However we believe our present results will be useful even if the work has to be redone with more detailed models, because a large part of the errors still remaining in the simulation are not attributable to the model, but to the initial state, and it is necessary to identify these errors before any firm conclusion can be drawn on this case. Of course, similar work will need to be performed on the whole PYREX data-set when the methodology is fully validated, before any conclusion can be made on the value of a particular parametrization.

Acknowledgments

The PYREX experiment was made possible by the participation of a large number of institutes and funding agencies. The participating institutes are CNRM, CRPE, LA, LAMP, LMD, LSEET, SA, EDF, for France, INM, UV, UIB, for Spain, and DLR, for Germany (see list of acronyms). Funding was provided by Météo-France, INM, INSU (ARAT and PAMOS Programs), CNES, EDF, DLR, and Région Midi-Pyrénées. Much technical help was provided by CEV, ENM, and the French and Spanish Airforce and Air Control authorities. We would like to express our gratitude to J.C. André, D. Cadet, D. Guédalia, and A. Ascaso Liria, for their help in the planing of this program. We also would like to express our deep appreciation to the many colleagues who have participated in the success of the experiment through enormous personnal commitment.

References

Attié, J.L., B. Benech, A. Druilhet, and P. Durand, 1991: *Comptes-rendus scientifiques des expériences aéroportées réalisées avec l'ARAT et le Merlin IV pendant PYREX.* Technical Report, Laboratoire d'Aérologie.

Attié, J.L., A. Druilhet, B. Bénech, P. Durand, and F. Saïd, 1992: Evaluation expérimentale des transferts verticaux d'énergie dans un flux d'air normal à une chaine de montagne. In *22nd International Conference on Alpine Meteorology*, pages 18–22.

Beau, I., 1992: *Evaluation des paramétrisations de l'effet orographique sous maille dans les modèles de circulation générale à l'aide de Péridot 10km.* Note de l'ENM.

Benech, B., A. Druilhet, R. Cordesse, B. Dartiguelongue, J. Fournet-Fayard, J.C. Mesnager, P. Durand, and A. Malaterre, 1987: Un dispositif expérimental utilisant des ballons plafonnants pour l'étude de la couche limite atmosphérique. *Adv. Space. Res.*, **7**, 77–83.

Benech, B., J.L.Attié, A. Blanchard, P. Bougeault, P. Cazaudarré, A. Druilhet, P. Durand, E. Koffi, P. Prudhomme, and D.S. Tannhauser, 1991: Observation of lee waves above the pyrénées (french spanish PYREX experiment). In *Technical Soaring, to appear.*

Benoit, R., 1992: Mass and momentum budgets from high-resolution upper-air soundings over the Pyrénées. In *22nd International Conference on Alpine Meteorology*, pages 8–13.

Bougeault, P., 1987: Simulations of orographic flows with a 10km-scale hydrostatic model. In *Workshop on Techniques for horizontal discretization in NWP models, European Center for Medium Range Weather Forecasts, Reading, 2-4 November 1987*, pages 229–248.

Bougeault, P. and R. Benoit, 1992: *La Base de Données PYREX.* Note du CNRM/GMME.

Bougeault, P., A. Jansa Clar, J.L. Attié, I. Beau, B. Bénech, R. Benoit, P. Bessemoulin, J.L. Caccia, B. Carissimo, J.L. Champeaux, M. Crochet, A. Druilhet, P. Durand, A. Elkhalfi, A. Genoves, M. Georgelin, K.P. Hoinka, V. Klaus, E. Koffi, V. Kotroni, C. Mazaudier, J. Pelon, M. Petitdidier, Y. Pointin, D. Puech, E. Richard, T. Satomura, J. Stein, and D. Tannhauser, 1992: The atmospheric momentum budget over a major mountain range: first results of the PYREX field program. *Annales Geophysicae*, . in preparation.

Bougeault, P., A. Jansa Clar, B. Benech, B. Carissimo, J. Pelon, and E. Richard, 1990: Momentum budget over the pyrénées: the PYREX experiment. *Bull. Amer. Meteor. Soc.*, **71**, 806–818.

Bougeault, P. and P. Lacarrère, 1989: Parameterization of orography-induced turbulence in a meso-beta scale model. *Mon. Wea. Rev.*, **117**, 1870–1888.

Bougeault, P. and C. Mercusot,1992: Atlas des analyses PERIDOT de l'expérience PYREX. Internal report, CNRM/GMME No 8.

Carissimo, B., J.M. Michelin, J. Jové, and D. Demengel, 1991: *Campagne PYREX: Atlas des données des stations du réseau EDF.* Note Technique EDF HE 33/91.13.

Champeaux, J.L. and P. Peris, 1991: *Expérience PYREX: Atlas des données sol de Météo-France.* Note de Travail du GMME.

Clark, T.L. and M.J. Miller, 1991: Pressure drag and momentum fluxes due to the Alps. II:representation in large-scale atmospheric models. *Quart. J. Roy. Meteor. Soc.*, **117**, 527–552.

Davies, H.C. and P.D. Phillips, 1985: Mountain drag along the Gotthard section during ALPEX. *J. Atmos. Sci.*, **42**, 2093–2109.

Durran, D., 1991: Orographic wave drag on the lower troposphere: the importance of trapped lee wave. In *8th Conference on Atmospheric waves and stability, Denver, 14-18 October, 1991*, pages 377–380.

Elkhalfi, A., 1992: *Comparaison hydrostatique non-hydrostatique avec le code MERCURE pour les écoulements sur relief comlexe.* Thèse de Doctorat de l'Ecole Centrale de Lyon.

Hoinka, K.P. and T.L. Clark, 1991: Pressure drag and momentum fluxes due to the Alps. I: comparison between numerical simulations and observations. *Quart. J. Roy. Meteor. Soc.*, **117**, 495–525.

Koffi, E., B. Benech, P. Bergue, B. Dartiguelongue, B. Dufour, D. Guedalia, G. Lachaud, N. Raynal, and C. Tarrieu, 1991: *Campagne PYREX: Traitement des données des ballons à volume constant relatives à l'étude du contournement.* Note du Laboratoire d'Aérologie.

Koffi, E., B. Benech, J. Dessens, P. Malaterre, J.C. Menager, G. Despaux, V. D. Pham, B. Campistron, and D. Tannhauser, 1991: *Campagne PYREX: Traitement des données des ballons à volume constant relatives à l'étude des ondes de sillage.* Note du Laboratoire d'Aérologie.

Lilly, D.K., 1972: Wave momentum flux - A GARP problem. *Bull. Amer. Meteor. Soc.*, **53**, 17–23.

Petitdidier, M., V. Klaus, F. Baudin, M. Crochet, G. Penazzi, and P. Quinty, 1986: *The INSU and DMN network of ST radars.* Handbook for MAP, **20**, INSU.

Puech, D., P. Bessemoulin, B. Dufour, and C. Tarrieu, 1991: *Catalogue des données du réseau sol 4M recueillies pendant l'expérience PYREX.* Note Interne du CNRM/GMEI.

Satomura, T. and P. Bougeault, 1992: Orographic wave drag during the PYREX experiment. In *Spring meeting of the Japanese Meteorological Society, 26-28 May, 1992,* page 282.

Stein, J., 1992: *Contribution à l'étude des régimes hydrostatiques d'écoulements orographiques.* Thèse de Doctorat, Université Paul Sabatier, Toulouse.

Stein, J., 1989: *Etude numérique de deux cas d'écoulement hydrostatique sur les Pyrénées, Rapport de Stage.* Ecole Nationale de la Météorologie. 189pp.

Tannhauser, D. and J. L. Attié, 1992: Optical and quantum mechanics analogs for trapped and leaky lee waves. In *22nd International Conference on Alpine Meteorology.*